Frontiers of Information Technology & Electronic Engineering
www.zju.edu.cn/jzus; engineering.cae.cn; www.springerlink.com
ISSN 2095-9184 (print); ISSN 2095-9230 (online)
E-mail: jzus@zju.edu.cn

Segmentation and focus-point location based on boundary analysis in forest canopy hemispherical photography*

Jia-yin SONG†, Wen-long SONG†‡, Jian-ping HUANG, Liang-kuan ZHU

(*College of Mechanical and Electrical Engineering, Northeast Forestry University, Harbin 150040, China*)

†E-mail: songjy@nefu.edu.cn; wls139@126.com

Received Apr. 14, 2016; Revision accepted July 14, 2016; Crosschecked July 26, 2016

Abstract: Analysis of forest canopy hemisphere images is one of the most important methods for measuring forest canopy structure parameters. In this study, our main focus was on using circular image region segmentation, which is the basis of forest canopy hemispherical photography. The boundary of a forest canopy hemisphere image was analyzed via histogram, rectangle, and Fourier descriptors. The image boundary characteristics were defined and obtained based on the following: (1) an edge model that contains three parts, i.e., step, ramp, and roof; (2) boundary points of discontinuity; (3) an edge that has a linear distribution of scattering points. On this basis, we proposed a segmentation method for the circular region in a forest canopy hemisphere image, fitting the circular boundary and computing the center and radius by the least squares method. The method was unrelated to the parameters of the image acquisition device. Hence, this study lays a foundation for automatically adjusting the parameters of high-performance image acquisition devices used in forest canopy hemispherical photography.

Key words: Fisheye lens, Least squares method, Image segmentation, Ecology in image processing, Hemispherical photography

http://dx.doi.org/10.1631/FITEE.1601169 **CLC number:** TP391.4; S758

1 Introduction

The forest canopy is the most direct and active interface layer with regard to interaction with the environment, and forest structural analysis is one of the key problems faced in ecological research. As research deepens, methods for measuring forest canopy structural parameters have been improved (Neumann and den Hartog, 1989; Sharma *et al.*, 2013; Huesca *et al.*, 2016) and ground measurement techniques have appeared. Among the various indirect techniques, the use of digital hemispherical photography (DHP) has soared in the past few years (Gonsamo and Pellikka, 2009; Liu C *et al.*, 2013; Brusa and Bunker, 2014; Zhao *et al.*, 2014; Liu Z *et al.*, 2015; Woodgate *et al.*, 2016), partly due to the advent of digital photography and continuing improvements in computer technology.

The DHP approach makes use of image acquisition hardware and computer software. The image acquisition hardware commonly consists of a camera with a fisheye lens and optional accessories (tripod, leveling mount, and remote controller). Images are stored commonly in compressed JPEG image format in the camera. The computer software is an image-analysis program for data manipulation and visualization. The advantages of using this approach are the affordability of the equipment, the ease of use, and the potential to allow integration over long periods from just one photograph (Mailly *et al.*, 2013).

‡ Corresponding author

* Project supported by the Fundamental Research Funds for the Central Universities, China (No. 2572014BB04), the National Natural Science Foundation of China (No. 31370710), and the Specialized Research Fund for the Doctoral Program of Higher Education of China (No. 20110062110002)

ORCID: Wen-long SONG, http://orcid.org/0000-0001-9729-7602

Forest canopy images can be collected by a circular 180° fisheye camera, and spherical projection is a simple and effective method to transform a circular 180° fisheye image into a perspective projection image (Schneider *et al.*, 2009; Ahmad *et al.*, 2014). Because the angle range of a fisheye lens is 0° to 180°, the image is known as a hemisphere image. The imaging process projects a point in a three-dimensional space onto a two-dimensional imaging plane through a coordinate transform.

Any point $\boldsymbol{p}$ in the world coordinate system $(X_{\mathrm{W}}, Y_{\mathrm{W}}, Z_{\mathrm{W}})$, which has an incidence angle of θ in the fisheye lens coordinate system $(X_{\mathrm{L}}, Y_{\mathrm{L}}, Z_{\mathrm{L}})$, must project to the point $\boldsymbol{p}'$ in the image plane (u, v) and the pixel coordinate system (x, y) (Fig. 1).

The forest canopy in the world coordinate system projects onto the image plane forming a circular region because of the size of the sensor and the shape of the fisheye lens (Fig. 2). The center of the circular region clearly is not the center of the image and the radius of the circular region is uncertain, as it is dependent on the image acquisition hardware. The DHP approach used to extract forest canopy structural parameters is based on the analysis of the circular region image. So, the performance of the hardware is very important. Fortunately, more and more high-performance cameras are available with the rapid development of digital photography technology.

Several hemispherical image-analysis programs have become available, such as Solarcalc 7.0 (Mailly *et al.*, 2013) and Can-Eye (http://www4.paca.inra.fr/can-eye). Commercial software is also available, e.g., Winscanopy 2012 (Regent Instruments, Canada) and HemiView (Delta-T Devices Ltd., UK). Table 1 summarizes the characteristics of the software.

We know that the imaging range of a photograph is decided not only by the optical center of the camera but also by the focal length. Different cameras with different fisheye lenses will have different imaging ranges. So, a fixed radius and center cannot meet the requirements of the hardware. Most importantly, the radius and the center cannot be found in the hardware specifications.

Automatic circle detection in digital images is an important issue of pattern recognition and computer vision. Some new methods are emerging, such as the power histogram based method (Yuan and Liu, 2015), center-based clustering method (Scitovski and Marošević, 2015), isophotes curvature

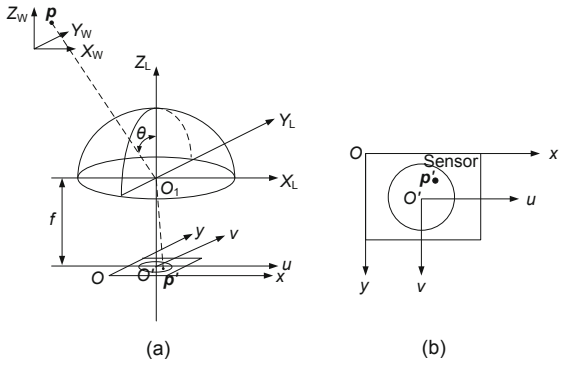

Fig. 1 Hemisphere imaging mechanism: (a) hemisphere imaging model; (b) image plane and pixel coordinate system

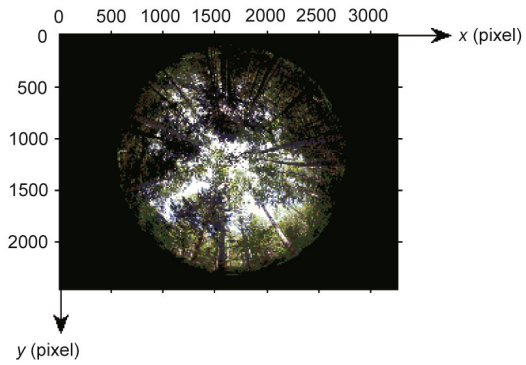

Fig. 2 Digital hemisphere canopy image

Table 1 Characteristics of hemispherical image-analysis programs

Software	Programming environment	Image segmentation
Solarcalc 7.0	BASIC	Draw radius (mouse position on image) or guess circle (fixed radius and center)
Can-Eye V6.314	MATLAB & C++	Input file of camera parameters (.xls)
Winscanopy 2012	Commercial secret	Matching with the hardware (fixed radius and mouse position on center)
HemiView	Commercial secret	Matching with the hardware (fixed optical center and radius)

analysis method (de Marco *et al.*, 2015), and isosceles triangles sampling method (Zhang *et al.*, 2016). The most widely used method is based on the circle Hough transform (Yao and Yi, 2016). However, all of the methods are limited to recognizing a circular target with the same trait and continuous boundary points such as coins, balls, plates, and logos. Meanwhile, the complex calculations limit the size of the image processed.

Clearly, there is a need to process large images. The target has a different trait whose boundary points are discretely distributed. So, the objective of our study is to propose an effective focus-point location segmentation algorithm to confirm the center and radius of a circular region image, which will provide technical support for the introduction of high-performance image acquisition equipment in DHP.

2 Image boundary analysis

A digital hemisphere canopy image is a 24-bit RGB full-color image. Usually, the noise content of a color image has the same characteristics in each color channel, but it is possible for color channels to be affected differently by the noise. Different noise levels are more likely to be caused by differences in the relative strength of illumination available to each of the color channels. Charge-coupled device (CCD) sensors are noisier at lower levels of illumination; therefore, the resulting red component of an RGB image tends to be noisier than the images of the other two components. In this situation, we use the blue component image and work on histogram analysis.

Fig. 2 shows an example that demonstrates the research process and result. It is a 24-bit RGB full-color image of 2448×3264 pixels in size.

For nearly bimodal distributions (Fig. 3), the intensity value of the valley could be used to identify a suitable bi-level threshold separating the object from the background.

Thresholding may be viewed as a statistical-decision theory problem whose objective is to minimize the average error incurred in assigning pixels to two groups. The global optimum thresholding using the Otsu method works well in situations where there is a reasonably clear valley between the modes of the histogram related to the objects and the background. According to the histogram threshold, the segmentation result is shown in Fig. 4b.

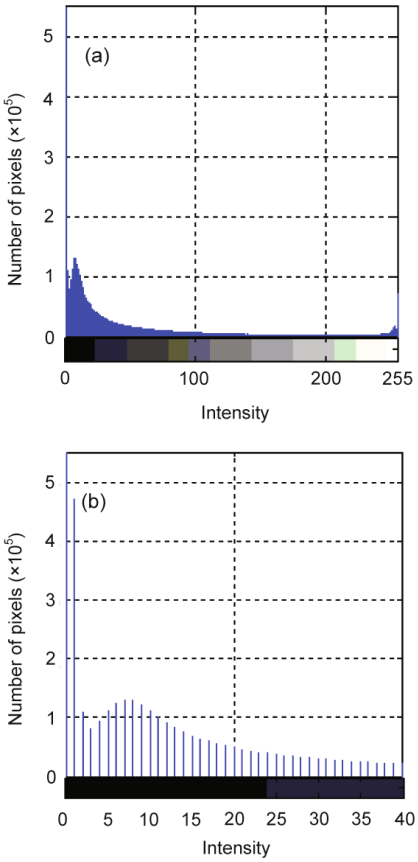

Fig. 3 Histogram of Fig. 2: (a) intensity levels in the range [0, 255]; (b) intensity levels in the range [0, 40]

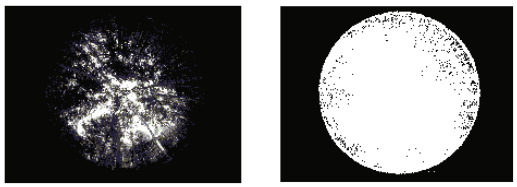

Fig. 4 Blue component image (a) and the segmentation result using a global threshold (b)

2.1 Shape feature

The rectangle degree is one of the image shape feature parameters which reacts to the filling level in the minimum enclosing rectangle. Denoting the area of the object by A_0, the area of the minimum enclosing rectangle by A_{MER}, the height of the minimum enclosing rectangle by H, and the width of the minimum enclosing rectangle by W, the rectangle degree

can be defined as follows:

$$K = \frac{A_0}{A_{\mathrm{MER}}} = \frac{A_0}{HW}. \tag{1}$$

When $K = \pi/4 = 0.7854$, the object is a circle. In Fig. 4b, $K = 0.7692$, $H = 2250$ pixels, and $W = 2235$ pixels. Thus, it is an approximate circle with an irregular boundary.

2.2 Edge models

Edge pixels are pixels at which the intensity of an image function changes abruptly. Fig. 5 shows a horizontal intensity profile of the image approximately through its center, including some isolated points.

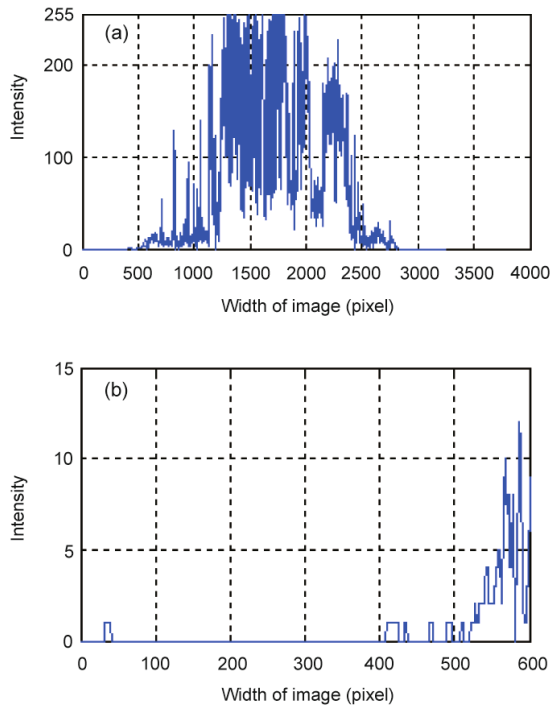

Fig. 5 Horizontal intensity profile through the center of the image (a) and that at the left boundary (b)

Considering the intensity at the left boundary, we draw the following conclusions:

1. The boundary points are discontinuous.

2. The image contains three types of edges, including the non-ideal models of step, ramp, and roof edge, from left to right.

3. The circular boundary would not be determined directly using edge detectors because of mode mixture.

2.3 Characteristics of boundary points

The performance of the Canny edge detector is superior in general to that of other edge detectors. The advantages of using this approach are a low error rate, well localized edge points, and single edge point response. Fig. 6 shows the result obtained with the Canny algorithm.

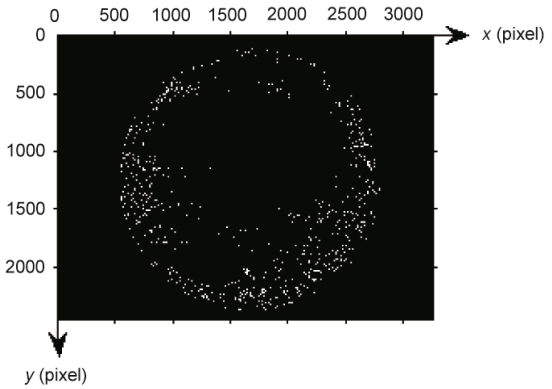

Fig. 6 Image obtained using the Canny algorithm

Fourier descriptors can be used to capture the gross essence of a boundary. Fig. 6 shows an N-point digital boundary in the xy-plane. The boundary itself can be represented as the sequence of coordinates $\boldsymbol{s}(k) = [x(k), y(k)]$ $(k = 0, 1, \ldots, N-1)$. Moreover, each coordinate pair can be treated as a complex number, i.e.,

$$s(k) = x(k) + \mathrm{j}y(k). \tag{2}$$

The discrete Fourier transform (DFT) of $s(k)$ is

$$a(u) = \sum_{k=0}^{N-1} s(k)\mathrm{e}^{-\mathrm{j}2\pi uk/N}, \tag{3}$$

where $u = 0, 1, \ldots, N-1$. The complex coefficients $a(u)$ are called the Fourier descriptors of the boundary. The inverse Fourier transform of these efficiently restores $s(k)$. That is,

$$s(k) = \frac{1}{N}\sum_{u=0}^{N-1} a(u)\mathrm{e}^{\mathrm{j}2\pi uk/N}, \tag{4}$$

where $k = 0, 1, \ldots, N-1$. Thus, the boundary description has been obtained in the rectangular coordinate system (Fig. 7). The position of the light source and the action of the light rays are shown clearly. We arrive at the following conclusions:

1. Circular external scattering points have a linear distribution where the positions are related to the light source location exit.

2. The center of the circle is not the image center.

3. We must remove the scattering points before computing the center and radius.

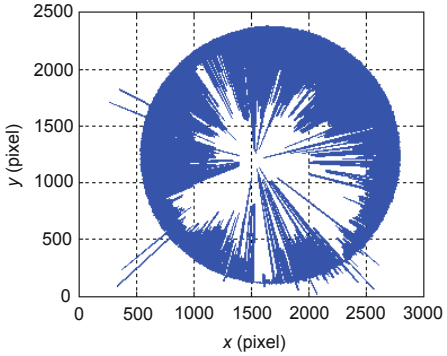

Fig. 7 Image obtained using the Fourier descriptors

3 Boundary fitting and segmentation

Based on the above analysis, the blue component of the digital hemisphere canopy image is transformed to a binary image using the threshold of the histogram (Lan and Zeng, 2013; Nafis *et al.*, 2013). The morphological opening would be used to remove the scattering points. The opening could remove a particular image detail that is smaller than the structural elements and, at the same time, ensure that it does not produce global geometric distortion (Kwak *et al.*, 2013; Bai, 2015).

3.1 Boundary point extraction technique

The set of all white pixels in a binary image is a complete morphological description of the image. Let the elements be represented by a set A whose elements are a tuple of the form (x, y), where x and y are coordinates of a white pixel in the image. Let the circular structuring elements be represented by a set B, of which the value of the structural parameter is two, and the origin is at the center of symmetry.

The opening of set A by structuring element B, denoted by $A \circ B$, is defined as follows:

$$A \circ B = (A \ominus B) \oplus B. \tag{5}$$

The opening A by B is the erosion of A by B, followed by a dilation of the result by B. The result of the opening is shown in Fig. 8a, and the set of all white pixels is represented by A. Suppose the elements in A are 8-connected boundaries, with each boundary enclosing a hole. Then the following procedure fills all the holes with 1 s:

$$X_k = (X_{k-1} \oplus B) \cap A^C, \ k = 1, 2, \ldots, \tag{6}$$

where B is the circle structuring element in Eq. (5). The algorithm terminates at iteration k if $X_k = X_{k-1}$. Set X_k then contains all the filled holes. The result of hole filling is shown in Fig. 8b, and the set of all white pixels is represented by $\hat{A}$. The boundary of set $\hat{A}$, denoted by $\beta(\hat{A})$, can be obtained by first eroding $\hat{A}$ by B and then performing the set difference between $\hat{A}$ and its erosion. That is,

$$\beta(\hat{A}) = \hat{A} - (\hat{A} \ominus B), \tag{7}$$

where B is the circle structuring element in Eq. (6). Fig. 8c shows the result of boundary extraction.

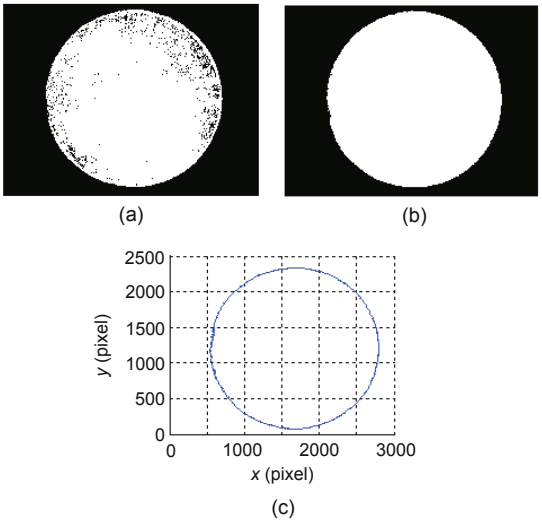

Fig. 8 Results of the opening (a), hole filling (b), and boundary extraction (c)

3.2 Focus-point location

The important aims of boundary analysis are to find the position of the center and obtain the radius accurately. On the premise of the known boundary point coordinates, the least squares method has been adopted (Ahn *et al.*, 2001; Chaudhuri, 2010; Kanatani and Rangarajan, 2011). Let (x_i, y_i) $(i =$

$1, 2, \ldots, n$) be n boundary points of object $\hat{A}$. We assume that (X_0, Y_0) are the center coordinates of the fitting circle. Therefore, the distance of a boundary point to the center of the fitting is

$$d_i = \sqrt{(x_i - X_0)^2 + (y_i - Y_0)^2}. \quad (8)$$

Thus, the square error will be

$$\delta_i = d_i^2 - R^2 = (x_i - X_0)^2 + (y_i - Y_0)^2 - R^2, \quad (9)$$

where R is the radius of the fitting circle. Then assuming $a = -2X_0$, $b = -2Y_0$, and $c = X_0^2 + Y_0^2 - R^2$, Eq. (9) becomes

$$\delta_i = x_i^2 + y_i^2 + ax_i + by_i + c. \quad (10)$$

Therefore, the square for all n points is

$$F = \sum_{i=1}^{n} \delta_i^2 = \sum_{i=1}^{n} (x_i^2 + y_i^2 + ax_i + by_i + c)^2. \quad (11)$$

Eq. (11) is a three-parameter (a, b, and c) function. We choose a, b, and c in such a way as to minimize the error δ_i^2. Thus, the optimal values of a, b, and c can be determined by solving the following three equations:

$$\frac{\partial F}{\partial a} = 0, \ \frac{\partial F}{\partial b} = 0, \frac{\partial F}{\partial c} = 0.$$

$\partial F/\partial a = 0$ gives

$$\sum_{i=1}^{n} 2x_i(x_i^2 + y_i^2 + ax_i + by_i + c) = 0. \quad (12)$$

$\partial F/\partial b = 0$ gives

$$\sum_{i=1}^{n} 2y_i(x_i^2 + y_i^2 + ax_i + by_i + c) = 0. \quad (13)$$

$\partial F/\partial c = 0$ gives

$$\sum_{i=1}^{n} 2(x_i^2 + y_i^2 + ax_i + by_i + c) = 0. \quad (14)$$

Solving Eqs. (12)–(14), we obtain Eqs. (15)–(17) (see the next page).

To test the effectiveness of the proposed techniques, we applied them to Fig. 8c and obtained $a = 3343.8$, $b = 2412.5$, and $c = 2\,981\,300$, while the radius of the fitting circle was 1126.5 pixels with (1671.9, 1206.3) as the center. The result of segmentation using the proposed method is shown in Fig. 9.

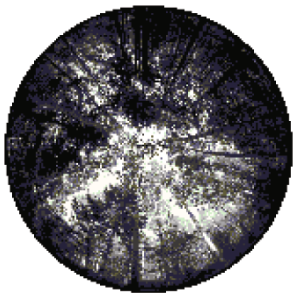

Fig. 9 Result of segmentation using the proposed method

3.3 Applications

We acquired hemispherical images using different cameras with fisheye lenses. To verify the algorithm, some clear boundary images were needed, but they were difficult to obtain because of the effects of a luminous beam. Some ideal images were acquired under an overcast sky and the proposed method was applied to those to calculate the center and the radius. The results were compared with manual measurements (Table 2).

The procedure of the manual measurements was as follows:

1. In Photoshop 8.0 the Circle Tool was selected to fit the circular region in the hemispherical photograph with white fill. Also, the same size image was filled with black.

2. According to the gray value, the center and radius were defined in MATLAB 7.0 based on the principle of rounded integers.

The center and the radius were obtained using different methods, giving the same results. We compared the center of the circle with the center of the image (Fig. 10). The results show that the smaller the image size, the larger the discrepancy between them. The center points of images having different sizes in the same equipment have a linear relationship.

On a clear day we used EOS 5D Mark II with EF 8–15 mm USM to acquire a forest canopy hemispherical image in the forest farm of the Northeast Forestry University. Images were acquired every hour from 1 pm to 5 pm because the intensity of the sunlight is approximately symmetrical during that period. A dual radiation meter was used to measure the photosynthetic photon flux at the spot for photography and the numerical values varied during image

$$a=\frac{\begin{vmatrix} n\sum_{i=1}^{n}x_i^2y_i+n\sum_{i=1}^{n}y_i^3-\sum_{i=1}^{n}(x_i^2+y_i^2)\sum_{i=1}^{n}y_i & n\sum_{i=1}^{n}x_i^3+n\sum_{i=1}^{n}x_iy_i^2-\sum_{i=1}^{n}(x_i^2+y_i^2)\sum_{i=1}^{n}x_i \\ n\sum_{i=1}^{n}y_i^2-\sum_{i=1}^{n}y_i\sum_{i=1}^{n}y_i & n\sum_{i=1}^{n}x_iy_i-\sum_{i=1}^{n}x_i\sum_{i=1}^{n}y_i \end{vmatrix}}{\begin{vmatrix} n\sum_{i=1}^{n}x_i^2-\sum_{i=1}^{n}x_i\sum_{i=1}^{n}x_i & n\sum_{i=1}^{n}x_iy_i-\sum_{i=1}^{n}x_i\sum_{i=1}^{n}y_i \\ n\sum_{i=1}^{n}x_iy_i-\sum_{i=1}^{n}x_i\sum_{i=1}^{n}y_i & n\sum_{i=1}^{n}y_i^2-\sum_{i=1}^{n}y_i\sum_{i=1}^{n}y_i \end{vmatrix}}, \tag{15}$$

$$b=\frac{\begin{vmatrix} n\sum_{i=1}^{n}x_i^2y_i+n\sum_{i=1}^{n}y_i^3-\sum_{i=1}^{n}(x_i^2+y_i^2)\sum_{i=1}^{n}y_i & n\sum_{i=1}^{n}x_i^3+n\sum_{i=1}^{n}x_iy_i^2-\sum_{i=1}^{n}(x_i^2+y_i^2)\sum_{i=1}^{n}x_i \\ n\sum_{i=1}^{n}x_iy_i-\sum_{i=1}^{n}x_i\sum_{i=1}^{n}y_i & n\sum_{i=1}^{n}x_i^2-\sum_{i=1}^{n}x_i\sum_{i=1}^{n}x_i \end{vmatrix}}{\begin{vmatrix} n\sum_{i=1}^{n}x_iy_i-\sum_{i=1}^{n}x_i\sum_{i=1}^{n}y_i & n\sum_{i=1}^{n}y_i^2-\sum_{i=1}^{n}y_i\sum_{i=1}^{n}y_i \\ n\sum_{i=1}^{n}x_i^2-\sum_{i=1}^{n}x_i\sum_{i=1}^{n}x_i & n\sum_{i=1}^{n}x_iy_i-\sum_{i=1}^{n}x_i\sum_{i=1}^{n}y_i \end{vmatrix}}, \tag{16}$$

$$c=-\frac{1}{n}\left[\sum_{i=1}^{n}(x_i^2+y_i^2)+a\sum_{i=1}^{n}x_i+b\sum_{i=1}^{n}y_i\right]. \tag{17}$$

Table 2 Comparison between instruments allowing center and radius calculation (unit: pixel)

Camera	Fish lens	Image size	Center (x_0, y_0)		Radius	
			Proposed	Manual	Proposed	Manual
Olympus E-500	ZUIKO DIGITAL 8 mm F1.8	450×508	(240.7352, 259.7178)	(241, 260)	185.4170	185
SIGMA SD1 Merrill	SIGMA 8 mm F3.5 EX	510×495	(280.5317, 243.8697)	(281, 244)	212.3763	212
Canon EOS 1DS Mark III	EF 8–15 mm USM	750×500	(374.0723, 252.6003)	(374, 253)	243.9720	244
iPhone 6S	OREA 0.42×	750×563	(368.8520, 346.7060)	(369, 347)	196.4401	196
Canon EOS 5D	SANYANG 8 mm F3.5 AE	800×533	(398.9051, 260.8717)	(399, 261)	260.2174	260
Nikon D300	Nikon 8 mm f/2.8	1000×945	(450.2681, 372.2106)	(450, 372)	273.8018	274
SONY A7R II	MADOKA 180	1000×1000	(498.5290, 496.4679)	(499, 496)	487.7187	488
Canon EOS 5D Mark III	EF 8–15 mm USM	1200×1200	(543.8606, 627.3253)	(544, 627)	493.2448	493
Canon EOS 5D Mark II	EF 8–15 mm USM	2784×1856	(1382.7000, 931.0079)	(1383, 931)	680.8354	681
Canon EOS 5D Mark II	EF 8–15 mm USM	4080×2720	(2026.0000, 1365.6000)	(2026, 1366)	990.8092	991
Canon EOS 5D Mark II	EF 8–15 mm USM	5616×3744	(2798.2000, 1878.5000)	(2798, 1879)	1366.7000	1367

acquisition. The images had the same size and different photo-sensibility (ISO 100–800). We calculated the center point and the distance to the standard center point (2026, 1366). Fig. 11 shows the results from the experiment on April 25, 2015.

In our study, although it was possible to calculate the center from all except from overexposed photographs, the result was affected by light intensity and photo-sensibility. This effect was uncertain and was related to the source location. However, when the photosynthetic photon flux was within the scope of 55 to 140 μmol/(m^2 · s) and the photo-sensibility from ISO100 to ISO250, the center was more consistent. This suggests that the light effect on the image had been minimized, so images could be collected in such conditions.

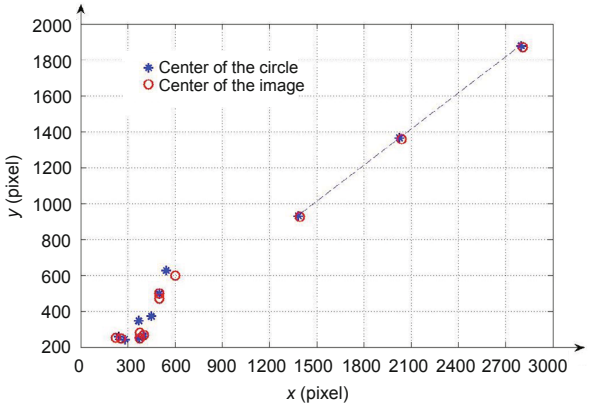

Fig. 10 Comparison between the center of the circle and the center of the image

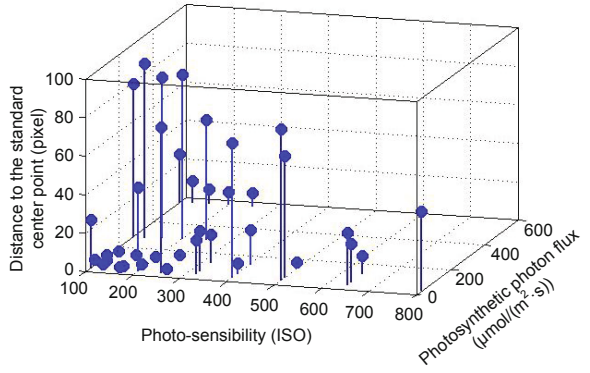

Fig. 11 Sample data from the experiment on April 25, 2015

4 Conclusions and future work

In this paper, we have proposed a method of segmentation based on boundary analysis. When projected onto an image through a fisheye lens based camera following a spherical projection model, the shape of the forest canopy image is circular. We presented a detailed analytical process for the boundary points, which had linear distributions under the influence of the light source location. Several points were outside the circular region. These were not the projected points of the forest canopy, but the scattering points of the light source. This explains why the boundary was an 'irregular' circle. To eliminate the scattering points, opening and hole filling were used, and the loss of several edge points yielded an error (Fig. 8b). The least squares method was applied to the fitting of the circular boundary to minimize the error. This method has proven its usability in terms of effective implementation and acceptable computing costs.

The validity of the algorithm was verified by comparing its results with those from manual measurements on different ideal images. Then the conditions suitable for collecting images were determined from the calculation of the center under different light conditions.

Our future work with respect to further development of techniques to extract forest canopy structure parameters is to apply a similar idea of image processing research to the forest canopy images that are collected by a fisheye lens in a high-performance camera. Another aspect that we are currently investigating is the relationship between the equipment parameters and the canopy structure parameters. We also intend to explore the possibility of characterizing error models of fisheye lenses and creating an error evaluation system.

References

Ahmad, A., Xavier, J., Santos-Victor, J., *et al.*, 2014. 3D to 2D bijection for spherical objects under equidistant fisheye projection. *Comput. Vis. Image Understand.*, **125**:172-183. http://dx.doi.org/10.1016/j.cviu.2014.04.004

Ahn, S.J., Rauh, W., Warnecke, H.J., 2001. Least-squares orthogonal distances fitting of circle, sphere, ellipse, hyperbola, and parabola. *Patt. Recogn.*, **34**(12):2283-2303. http://dx.doi.org/10.1016/S0031-3203(00)00152-7

Bai, X., 2015. Morphological infrared image enhancement based on multi-scale sequential toggle operator using opening and closing as primitives. *Infrared Phys. Technol.*, **68**:143-151. http://dx.doi.org/10.1016/j.infrared.2014.11.015

Brusa, A., Bunker, D.E., 2014. Increasing the precision of canopy closure estimates from hemispherical photography: blue channel analysis and under-exposure. *Agr. Forest Meteorol.*, **195-196**:102-107. http://dx.doi.org/10.1016/j.agrformet.2014.05.001

Chaudhuri, D., 2010. A simple least squares method for fitting of ellipses and circles depends on border points of a two-tone image and their 3-D extensions. *Patt. Recogn. Lett.*, **31**(9):818-829. http://dx.doi.org/10.1016/j.patrec.2010.01.009

de Marco, T., Cazzato, D., Leo, M., *et al.*, 2015. Randomized circle detection with isophotes curvature analysis. *Patt. Recogn.*, **48**(2):411-421. http://dx.doi.org/10.1016/j.patcog.2014.08.007

Gonsamo, A., Pellikka, P., 2009. The computation of foliage clumping index using hemispherical photography. *Agr. Forest Meteorol.*, **149**(10):1781-1787. http://dx.doi.org/10.1016/j.agrformet.2009.06.001

Huesca, M., García, M., Roth, K.L., *et al.*, 2016. Canopy structural attributes derived from AVIRIS imaging spectroscopy data in a mixed broadleaf/conifer forest. *Remote Sens. Environ.*, **182**:208-226. http://dx.doi.org/10.1016/j.rse.2016.04.020

Kanatani, K., Rangarajan, P., 2011. Hyper least squares fitting of circles and ellipses. *Comput. Stat. Data Anal.*, **55**(6):2197-2208. http://dx.doi.org/10.1016/j.csda.2010.12.012

Kwak, K., Yoon, U., Lee, D.K., *et al.*, 2013. Fully-automated approach to hippocampus segmentation using a graph-cuts algorithm combined with atlas-based segmentation and morphological opening. *Magn. Reson. Imag.*, **31**(7):1190-1196. http://dx.doi.org/10.1016/j.mri.2013.04.008

Lan, J., Zeng, Y., 2013. Multi-threshold image segmentation using maximum fuzzy entropy based on a new 2D histogram. *Optik Int. J. Light Electon Opt.*, **124**(18):3756-3760. http://dx.doi.org/10.1016/j.ijleo.2012.11.023

Liu, C., Kang, S., Li, F., *et al.*, 2013. Canopy leaf area index for apple tree using hemispherical photography in arid region. *Sci. Horticult.*, **164**:610-615. http://dx.doi.org/10.1016/j.scienta.2013.10.009

Liu, Z., Wang, C., Chen, J.M., *et al.*, 2015. Empirical models for tracing seasonal changes in leaf area index in deciduous broadleaf forests by digital hemispherical photography. *Forest Ecol. Manag.*, **351**:67-77. http://dx.doi.org/10.1016/j.foreco.2015.05.005

Mailly, D., Turbis, S., Chazdon, R.L., 2013. SOLARCALC 7.0: an enhanced version of a program for the analysis of hemispherical canopy photographs. *Comput. Electron. Agr.*, **97**:15-20. http://dx.doi.org/10.1016/j.compag.2013.06.004

Nafis, U.K., Arya, K.V., Pattanaik, M., 2013. Histogram statistics based variance controlled adaptive threshold in anisotropic diffusion for low contrast image enhancement. *Signal Process.*, **93**(6):1684-1693. http://dx.doi.org/10.1016/j.sigpro.2012.09.009

Neumann, H.H., den Hartog, G., 1989. Leaf area measurements based on hemispheric photographs and leaf-litter collection in a deciduous forest during autumn leaf-fall. *Agr. Forest Meteorol.*, **45**(3-4):325-345. http://dx.doi.org/10.1016/0168-1923(89)90052-X

Schneider, D., Schwalbe, E., Maas, H.G., 2009. Validation of geometric models for fisheye lenses. *ISPRS J. Photogr. Remote Sens.*, **64**(3):259-266. http://dx.doi.org/10.1016/j.isprsjprs.2009.01.001

Scitovski, R., Marošević, T., 2015. Multiple circle detection based on center-based clustering. *Patt. Recogn. Lett.*, **52**:9-16. http://dx.doi.org/10.1016/j.patrec.2014.09.010

Sharma, R.C., Kajiwara, K., Honda, Y., 2013. Estimation of forest canopy structural parameters using kernel-driven bi-directional reflectance model based multi-angular vegetation indices. *ISPRS J. Photogr. Remote Sens.*, **78**:50-57. http://dx.doi.org/10.1016/j.isprsjprs.2012.12.006

Woodgate, W., Armston, J.D., Disney, M., *et al.*, 2016. Quantifying the impact of woody material on leaf area index estimation from hemispherical photography using 3D canopy simulations. *Agr. Forest Meteorol.*, **226-227**:1-12. http://dx.doi.org/10.1016/j.agrformet.2016.05.009

Yao, Z., Yi, W., 2016. Curvature aided Hough transform for circle detection. *Exp. Syst. Appl.*, **51**:26-33. http://dx.doi.org/10.1016/j.eswa.2015.12.019

Yuan, B., Liu, M., 2015. Power histogram for circle detection on images. *Patt. Recogn.*, **48**(10):3268-3280. http://dx.doi.org/10.1016/j.patcog.2015.01.003

Zhang, H., Wiklund, K., Andersson, M., 2016. A fast and robust circle detection method using isosceles triangles sampling. *Patt. Recogn.*, **54**:218-228. http://dx.doi.org/10.1016/j.patcog.2015.12.004

Zhao, D., Lv, M., Wang, P., *et al.*, 2014. Can the plant area index of a submerged vegetation canopy be estimated using digital hemispherical photography? *Agr. Forest Meteorol.*, **192-193**:69-77. http://dx.doi.org/10.1016/j.agrformet.2014.03.008